Available online at www.sciencedirect.com
SCIENCE DIRECT®
European Journal of Mechanics B/Fluids 23 (2004) 199–208

# Vortex-induced travelling waves along a cable

Matteo Luca Facchinetti [a,b], Emmanuel de Langre [a,*], Francis Biolley [b]

[a] *Département de mécanique, LadHyX–CNRS, École polytechnique, 91128 Palaiseau, France*
[b] *IFP–1, 4, av. de Bois Préau, 92852 Rueil-Malmaison, France*

Received 7 April 2003; accepted 24 April 2003

**Abstract**

We investigate the vortex-induced vibrations (VIV) of a very slender cable subjected to a stationary uniform cross-flow, using a travelling wave approach. A phenomenological model of the near wake based on van der Pol oscillators is developed and tested in comparison with numerical simulations and experimental data. A selection criterion for vortex-induced waves (VIW) is established: the fluid selects the frequency, according to Strouhal's law, and the structure fixes the wavenumber, as dictated by its dispersion relation.


*Keywords:* Fluid–structure interaction; Vortex-Induced Vibrations (VIV); Vortex-Induced Waves (VIW); Wake oscillator; Van der Pol

## 1. Introduction

Vortex-induced vibration (VIV) is a fluid-structure interaction phenomenon which affects several kinds of structures subjected to wind or water currents. In the recent development of oil fields in deep ocean, cables and risers of large length-to-diameter aspect ratio and complex geometry are used, and VIV remains a challenging problem. As the aspect ratio exceeds $10^3$, vortex-induced motion may damp out before reaching the structure ends. Vandiver [1] and Moe et al. [2] discuss the application of the infinite length structure model by defining a wave propagation parameter. Moreover, the particular boundary conditions at the sea bed and at the sea surface, and the possible presence of intermediate buoyancy modules, make wave transmission and reflection ineffective. Alexander [3] qualitatively observed propagating waves along a towed oceanographic cable, which is a configuration very similar to that of a riser disconnected to the well head. Karniadakis et al. [4–6] discuss on standing/travelling wave behavior of cables and beams depending on boundary conditions, simulating the flow field by DNS at low Reynolds number.

Here we analyze the dynamics of very slender complex structures submitted to VIV using a travelling wave approach and introducing the concept of vortex-induced wave (VIW). A phenomenological model of the near wake based on van der Pol wake oscillators is used, allowing an analytical approach to the problem and overcoming the computational limits of flow-field numerical model in describing high aspect ratio domains at high Reynolds number. Considering a cable of infinite length, a selection criterion for VIW frequency and wavenumber is established by analytical arguments in Section 2, then validated by numerical simulations and against DNS computations in Section 3, and by comparison to experiments in Section 4. Discussion follows in Section 5.

* Corresponding author.
*E-mail address:* delangre@ladhyx.polytechnique.fr (E. de Langre).

0997-7546/$ – see front matter 
doi:10.1016/j.euromechflu.2003.04.004

## 2. Model

### 2.1. Motion of the structure

Let us consider a very slender straight cable with diameter $D$ and constant axial tension $T$, subject to a stationary and uniform flow of free stream velocity $U$, Fig. 1. The dynamics of a such a structure experiencing VIV may be described by a classical cable model [7,8]. We consider the structure diameter $D$ as a reference length scale and the Strouhal frequency $\omega_f = 2\pi S_t U/D$, $S_t$ being the Strouhal number, as a reference time scale. In the absence of fluid forces, the in-plane cross-flow deflection $y(z,t)$ of the cable is described by the dimensionless wave equation

$$\frac{\partial^2 y}{\partial t^2} + \left(\zeta + \frac{\gamma}{\mu}\right)\frac{\partial y}{\partial t} - c^2\frac{\partial^2 y}{\partial z^2} = 0. \tag{1}$$

The dimensionless phase velocity is $c = \sqrt{T/m}/(\omega_f D)$, where the mass per unit length $m$ includes the quiescent fluid added mass. The linear damping model distinguish the structural contribution $\zeta$ from the fluid added damping $\gamma/\mu$. The coefficient $\mu = m/\rho D^2$ is the mass ratio and $\gamma$ is a stall parameter derived considering the variation of the incident angle of the relative flow for an oscillating structure [9–11].

### 2.2. Wake dynamics

The near wake vortex street behind the structure is described by a phenomenological model. At each spanwise location, the fluctuating nature of vortex shedding is modelled by a wake oscillator, Fig. 1. For a slender structure a continuous distribution of wake oscillators, arranged along the structure axis, is applied. Following [12–14], this model makes use of non-linear van der Pol oscillators and reads

$$\frac{\partial^2 q}{\partial t^2} + \varepsilon\left(q^2 - 1\right)\frac{\partial q}{\partial t} + q = 0. \tag{2}$$

The dimensionless variable $q(z,t)$ describes any fluctuating variable of the near wake. It may be associated with the fluctuating lift coefficient on the structure, as in most of the wake oscillator models in the literature since [15]. Since the vortex shedding frequency is taken as the reference time scale, the basic angular frequency of the van der Pol oscillator is one. Note that for $0 < \varepsilon \ll 1$, Eq. (2) is known to provide a stable quasi-harmonic oscillation of normalized amplitude $q_o = 2$ at the normalized vortex shedding angular frequency of one.

### 2.3. Coupling

We now propose to couple the dynamics of the wake and of the structure, Eqs. (1) and (2), as follows

$$\frac{\partial^2 y}{\partial t^2} + \left(\zeta + \frac{\gamma}{\mu}\right)\frac{\partial y}{\partial t} - c^2\frac{\partial^2 y}{\partial z^2} = Mq, \tag{3}$$

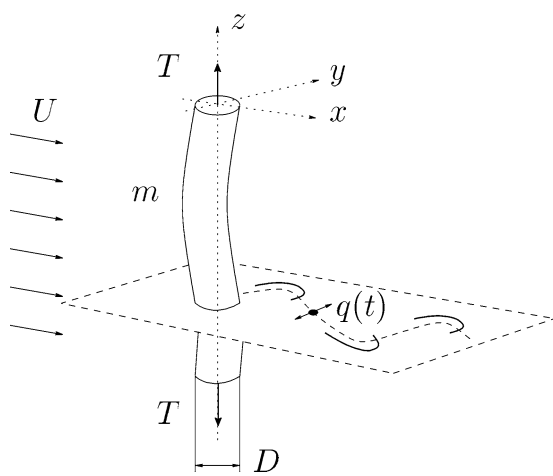


Fig. 1. Fluid–structure model: a very slender tensioned cable in stationary uniform flow.

$$\frac{\partial^2 q}{\partial t^2} + \varepsilon\left(q^2 - 1\right)\frac{\partial q}{\partial t} + q = A\frac{\partial^2 y}{\partial t^2}. \tag{4}$$

Here, the hydrodynamic actions on the structure are represented in three terms: (a) the quiescent added mass effect is directly included in the mass ratio $\mu$; (b) the damping associated to the flow is modelled by the added damping $\gamma$; (c) the fluctuating force due to the wake dynamics is modelled by the right-hand side forcing term of Eq. (3). The transverse vortex force exerted by the fluid on the structure is considered as a linear fluctuating lift. The wake variable $q$ is then interpreted as a normalized lift coefficient, $q = 2C_L/C_{Lo}$, where $C_{Lo}$ is the lift coefficient amplitude on a fixed structure experiencing vortex shedding. Thus, the dimensionless fluid forcing term is expressed by $Mq$, where $M = C_{Lo}/(16\pi^2 S_t^2 \mu)$ is a mass number. Conversely, the action of the structure on the fluid near wake is considered as linear and purely inertial, $A$ being the scaling parameter. This is shown to describe the main features of VIV phenomenology, such as Griffin plots and lock-in domains [16,19].

### 2.4. Parameters

The parameters of the structure equation (3) are directly defined by the specific properties of the physical system, namely the mass ratio $\mu$ and the reduced damping $\zeta$, the parameter $M$ depending only on the mass ratio $\mu$. For cylinders, we assume $S_t = 0.2$ in the sub-critical range, $300 < R_e < 1.5 \times 10^5$, and $C_{Lo} = 0.3$ over a large range of $R_e$ [9,17]. The only remaining parameter to be determined is the fluid added damping coefficient $\gamma$, which has been directly related to the mean sectional drag coefficient of the structure through $\gamma = C_D/(4\pi S_t)$ [9]. For oscillating cylinders, we assume here a constant drag coefficient $C_D = 2.0$ [9,17], from which we deduce $\gamma = 0.8$.

The fluid equation (4) requires the knowledge of two parameters: $\varepsilon$ and $A$. Their values are set by considering the effects of an imposed motion of the structure on the local near wake dynamics. Experiments since [18] show that the lift force acting on the structure, namely $q$, is magnified by an imposed structure motion $y$. The fluid model is forced by a harmonic motion of dimensionless amplitude $y_o$ and unit angular frequency, $y = y_o \cos(t)$, in perfect resonance condition with the Strouhal frequency. Enforcing the hypothesis of harmonicity and frequency synchronization, the response of the wake oscillator is sought in the form $q = q_o \cos(t + \psi)$, where $q_o$ and $\psi$ are time-independent amplitude and phase, respectively. Substituting in the fluid model and considering only the main harmonic contribution of the non-linearities, elementary algebra yields the amplitude of the transfer function of the wake oscillator. The lift magnification factor with respect to the case of a stationary structure experiencing vortex shedding, $K = C_L/C_{Lo} = q_o/2$, then reads [16,19]

$$K = \left(\frac{X}{36}\right)^{1/3} + \left(\frac{4}{3X}\right)^{1/3} \quad \text{with } X = \left(9\frac{A}{\varepsilon}y_o\right) + \sqrt{\left(9\frac{A}{\varepsilon}y_o\right)^2 - 48}. \tag{5}$$

The combined parameter $A/\varepsilon$ may now be chosen by matching the model response (5) to experimental data of lift magnification found in the literature. The value of $A/\varepsilon = 40$ is proposed from a least squares interpolation, Fig. 2. The respective values of $A$ and $\varepsilon$ may be derived separately from experimental considerations [16,19], but the value of the ratio $A/\varepsilon$ is sufficient in the present paper.

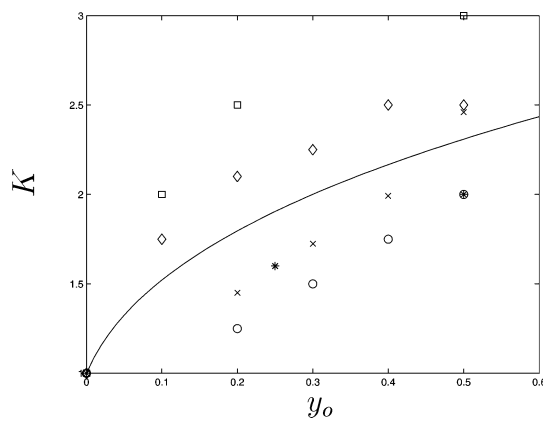


Fig. 2. Lift magnification $K$ as a function of the imposed structure motion amplitude $y_o$. —, model response (5) fitted to experimental data: ◇, [18]; ×, [20]; *, [21]; □, [22]; ○, [17]. Model parameters: $A/\varepsilon = 40$.

### 2.5. Wave dynamics

The dynamics of the system (3), (4) is now analyzed by searching for solutions in the form of harmonic travelling waves

$$y(z,t) = y_o\, \mathrm{e}^{\mathrm{i}(kz-\omega t-\varphi)}, \qquad q(z,t) = q_o\, \mathrm{e}^{\mathrm{i}(kz-\omega t)}, \tag{6}$$

where the structure and fluid variables admit a common real angular frequency $\omega$ and a real wavenumber $k$, time-independent real amplitudes $y_o$, $q_o$ and a relative phase $\varphi$. After substitution of (6) in system (3), (4), to the leading order in frequency, elementary algebra yields

$$\begin{bmatrix} \mathsf{D}_S(\omega,k) & -M\,\mathrm{e}^{+\mathrm{i}\varphi} \\ \omega^2 A\,\mathrm{e}^{-\mathrm{i}\varphi} & \mathsf{D}_F(\omega,k,q_o) \end{bmatrix} \begin{pmatrix} y_o \\ q_o \end{pmatrix} = 0, \tag{7}$$

where the diagonal terms $\mathsf{D}_S$ and $\mathsf{D}_F$ are the dispersion relations of the structure and the fluid, respectively

$$\mathsf{D}_S(\omega,k) = -\omega^2 - \mathrm{i}\left(\zeta + \frac{\gamma}{\mu}\right)\omega + c^2k^2 = 0, \tag{8}$$

$$\mathsf{D}_F(\omega,k;q_o) = -\omega^2 - \mathrm{i}\varepsilon\left(1 - \frac{q_o^2}{4}\right)\omega + 1 = 0. \tag{9}$$

Seeking for non-trivial neutral waves ($\omega$ real, $k$ real), the determinant of the coefficient matrix of the system (7) is set equal to zero, leading to the non-linear dispersion relation of the coupled fluid–structure system

$$\mathsf{D}_{FS}(\omega,k;q_o) = \mathsf{D}_S(\omega,k)\mathsf{D}_F(\omega,k;q_o) + AM\omega^2 = 0. \tag{10}$$

Setting the imaginary part of (10) equal to zero yields an equation for the wave amplitude $q_o$, which reads

$$\frac{q_o^2}{4} = 1 + \frac{AM}{\varepsilon}\frac{(\zeta+\gamma/\mu)\omega^2}{[c^2k^2-\omega^2]^2 + [(\zeta+\gamma/\mu)\omega]^2}. \tag{11}$$

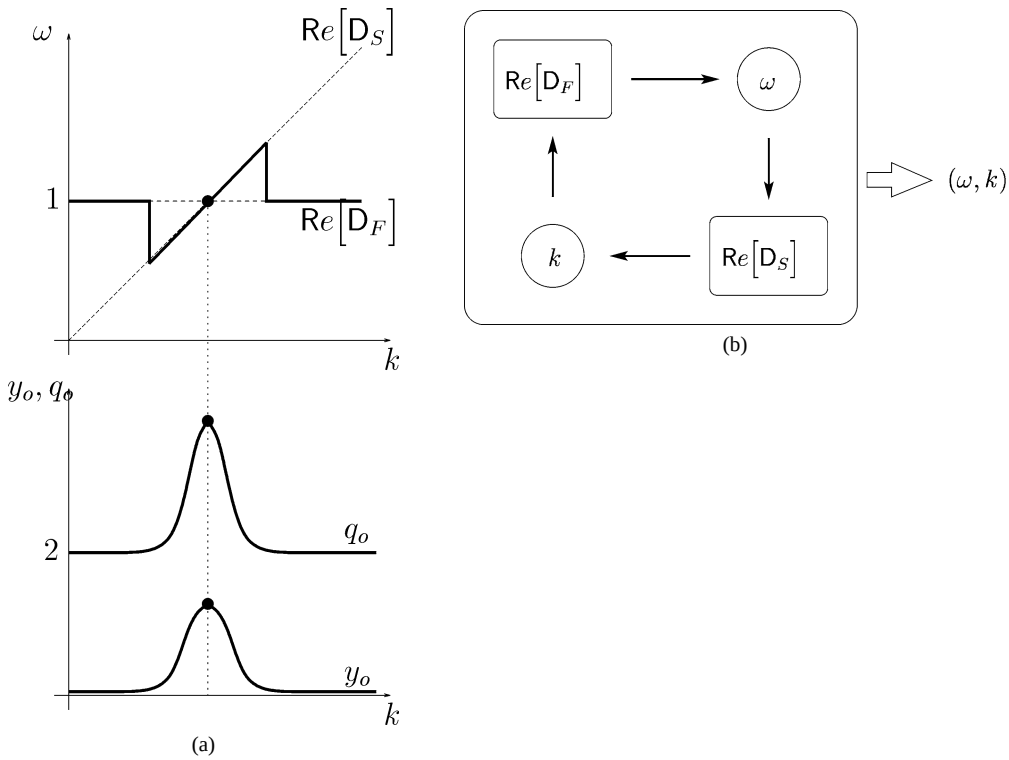


Fig. 3. Solution of the coupled system (3), (4): (a) - -, fluid and structure undamped dispersion relations; —, infinite sets $(\omega, k; q_o)$ satisfying Eqs. (11), (12); •, wave of maximum amplitude. (b) Selection scheme for the couple $(\omega, k)$.

Setting the real part of (10) equal to zero leads to the a bi-cubic polynomial of $\omega$ as a function of $k$, namely

$$\omega^6 - \left[1 + 2c^2k^2 - (\zeta + \gamma/\mu)^2 - AM\right]\omega^4 - \left[-2c^2k^2 + (\zeta + \gamma/\mu)^2 - c^4k^4 + AMc^2k^2\right]\omega^2 - \left[c^4k^4\right] = 0. \tag{12}$$

Eqs. (11), (12) are satisfied by infinite sets $(\omega, k; q_o)$, as sketched in Fig. 3(a). For a structure of finite length, the selection of particular values would be given by the boundary conditions. Here, for an infinite medium, a selection criterion needs to be established: we consider here the wave of maximum wake and cable amplitude, $q_o$ and $y_o$, defined by the resonance condition

$$\mathrm{Re}[\mathsf{D}_S] = -\omega^2 + c^2k^2 = 0, \qquad \mathrm{Re}[\mathsf{D}_F] = -\omega^2 + 1 = 0. \tag{13}$$

These equations do not depend on the values of $\varepsilon$ and $A$ and depend only on the mass-stiffness properties of the fluid–structure model (34). They define the intersection of the undamped dispersion relations of the structure and the fluid: in the $(\omega, k)$ plane, this defines the wave angular frequency and wavenumber, Fig. 3(b).

From a physical point of view, uneffective boundary conditions allow any couple $(\omega, k)$ satisfying the structure dispersion relation with no preference. The fluid is therefore able to select autonomously the Strouhal frequency and the synchronization assumption allows the structure to fix the wavenumber, as dictated by its own dispersion relation. Roughly speaking, the fluid is the only real source of the common VIW frequency, while the structure fixes the common wavenumber.

## 3. Numerical simulations

The selection criterion of VIW features based on the maximum wave amplitude, and thus considering the intersection of the structure and fluid undamped dispersion relations, is now validated by numerical simulations. The dynamical system (3), (4) is integrated by applying a standard centered finite difference method in time and space, using a second order accurate time-space explicit scheme. We model a typical marine cable of mass ratio $\mu = 1.785$ and constant phase velocity $c = 5$, subjected to VIV in the laminar regime. From DNS computations at $R_e = 100$ [4], we consider $S_t = 0.16$ and $C_{Lo} = 0.34$. Initial conditions are chosen in order to model the onset of Bénard–von Kármán vortex street as the stream flow is switched on from rest: random noise of amplitude $\mathrm{O}(10^{-3})$ is considered for the fluid, as a perturbation of the unstable fixed point for the spatially interacting van der Pol oscillators, whereas a static rest position is assumed for the structure. In order to model a structure of infinite length, absorbing boundary conditions are applied, using a mechanical impedance condition, $\partial y/\partial_t = \pm c\partial y/\partial_z$ [7], whereas for the fluid the regularity condition $\partial^2 q/\partial z^2 = 0$ is set. As shown in the spatio–temporal evolution in Fig. 4, waves with the predicted frequency $\omega = 1$, wavenumber $k = \omega/c = 0.2$ and amplitude $q_o = 0.22$ radiate throughout both spanwise boundaries, and a source point appears in the domain. This confirms the selection of the VIW frequency by Strouhal's law and the wavenumber by the structure undamped dispersion relation.

Considering a portion of cable with periodic boundary conditions, the spatio–temporal evolution of the structure transverse displacement $y(z, t)$ obtained by numerical simulations of the system (3), (4) is now compared to VIV numerical simulations, where the entire flow field is computed by DNS [4], Fig. 5. In both results, the observed frequency is predicted by Strouhal's law, and the wavenumber of stationary and travelling waves is that resulting from the cable constant phase velocity, here $c = 2$. Moreover, the phenomenological model of the near wake used here is found able to describe stationary waves, travelling waves and transients as observed by DNS computations in [4].

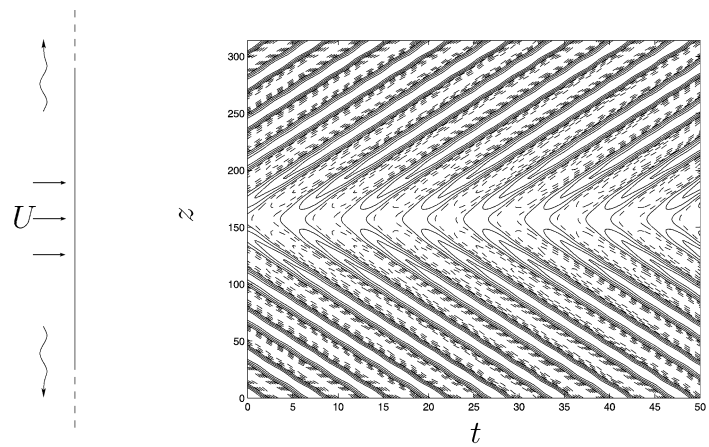


Fig. 4. Spatio–temporal evolution of the system (3), (4) showing vortex-induced travelling waves (VIW). Iso-lines of structure transverse displacement $y = -0.25 : 0.05 : +0.25$; - -, $y < 0$; —, $y > 0$.

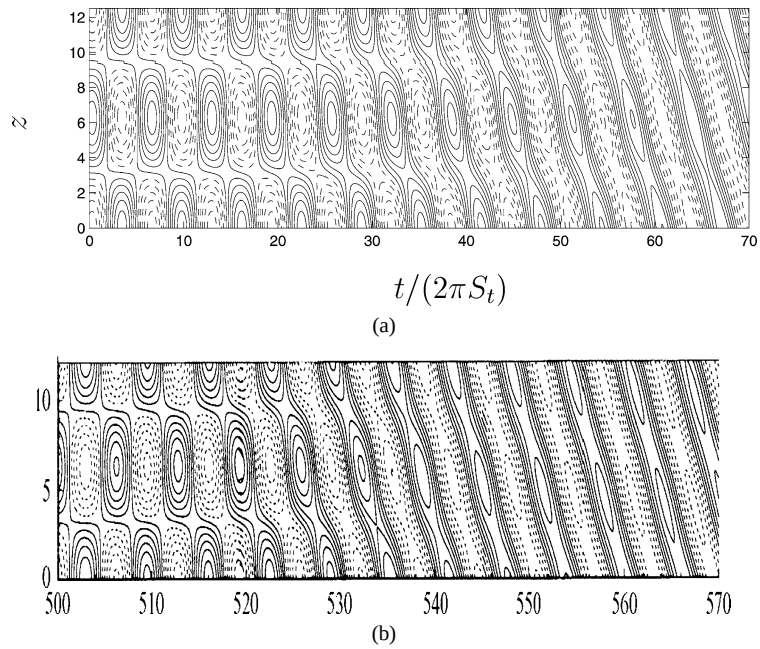


Fig. 5. Transverse displacement $y(z,t)$ of a cable submitted to VIV: (a) numerical simulation of system (3), (4); (b) DNS computations [4].

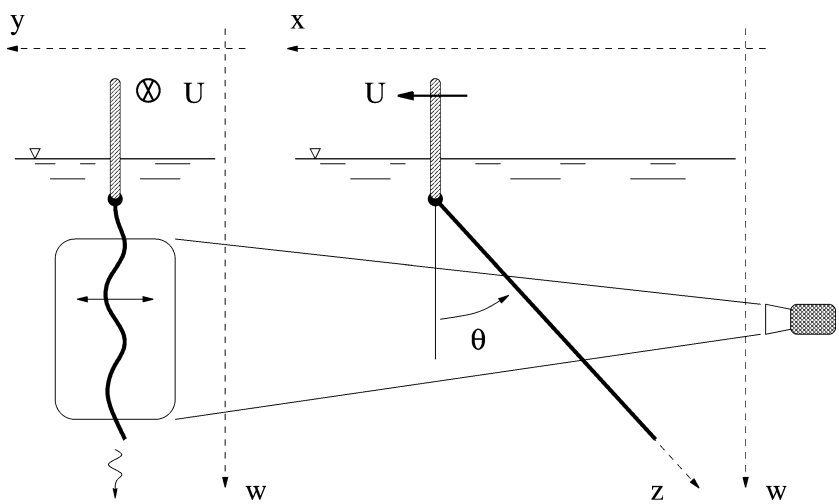


Fig. 6. Experimental set-up.

## 4. Experiments

### *4.1. Set-up*

The selection criterion of VIW features based on the maximum wave amplitude, considering the intersection of the structure and fluid undamped dispersion relations, is now validated experimentally. A long flexible cable is towed in a water tank and submitted to vortex shedding excitation, experiencing VIW, Fig. 6. A stationary digital video camera is aligned with the vertical towing plane: the movie thus obtained is processed in order to correct for parallax and perspective aberration, yielding the spatio–temporal evolution of the cable transverse displacement, $y(z,t)$. The upper end of the cable is connected to a towing carriage under the free surface to avoid any interface effect. The lower end is unrestrained in order to model a partially non-reflecting boundary condition through the effect of vanishing tension. The cable has a mass ratio of $\mu = 1.625$ and an aspect ratio of $L/D = 250$. The experiments are carried out at Reynolds number of the order of 100. A spatio–temporal evolution

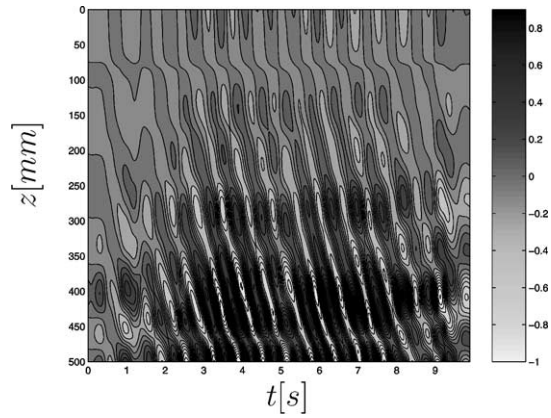


Fig. 7. VIW travelling downwards on a cable: experimental data of the spatio–temporal evolution of the cable transverse displacement $y(z,t)$.

graph of the towed cable transverse displacement $y(z,t)$ shows definite evidence of VIW travelling downwards on the towed cable, Fig. 7.

### 4.2. Model

According to [23,24], the vortex-induced motion of the towed cable may be considered as a transverse perturbation of the stationary vertical towing equilibrium, Fig. 8. The bending angle $\theta$ results from the balance of fluid and gravity forces, leading to a spanwise linear variable tension in the cable, namely a constant inclination. Fluid forces are reduced to a drag force $S_N$ and a viscous friction $S_T$, which read [25,9]

$$S_N = \frac{1}{2}\rho(U\cos\theta)^2 DC_D, \qquad S_T = \frac{1}{2}\rho U^2 \sin\theta\pi DC_F, \tag{14}$$

where $C_D = 4.5$ is the sectional drag coefficient of the vibrating cable [9] and $C_F = 0.083$ is the surface friction coefficient [25]. Considering the apparent cable mass per unit length in water, $m_e = 6\times10^{-4}$ kg/m, the static equilibrium in the direction normal to the cable yields the bending angle $\theta$

$$\cos^2\theta = \frac{-1+\sqrt{1+4G}}{2G}, \quad G = \left(\frac{1}{2}\frac{\rho DL_r}{m_e}C_D F_r^2\right)^2, \tag{15}$$

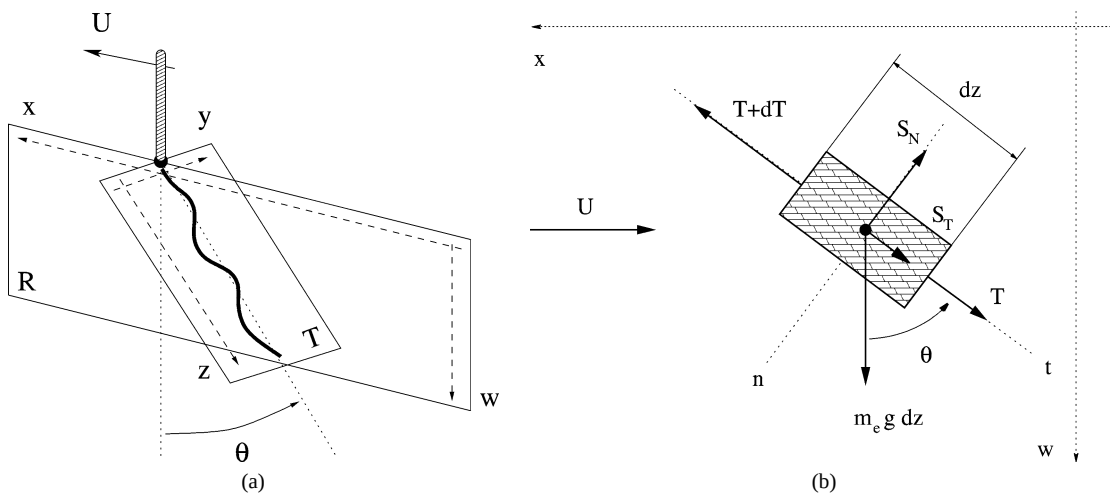


Fig. 8. (a) Cable motion: R, vertical towing plan of the static equilibrium; T, transverse plan of the VIW. (b) Cable static equilibrium in the vertical towing plan.

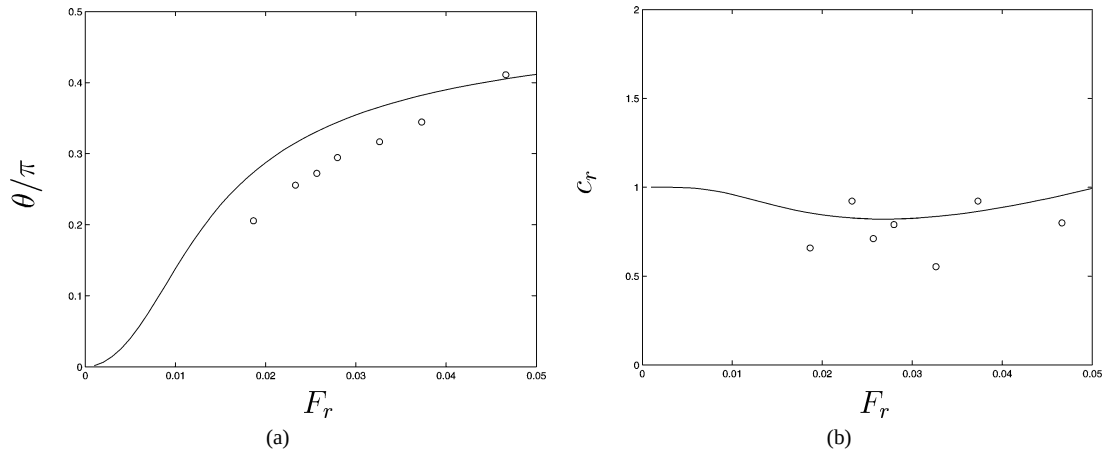


(a) (b)

Fig. 9. (a) Inclination angle $\theta$ as a function of the Froude number $F_r$: ∘, experiments; —, Eq. (15). (b) Non-dimensional phase velocity $c_r$ as a function of the Froude number $F_r$: ∘, experiments; —, Eq. (17).

where $F_r = U/\sqrt{gL_r}$ is the Froude number and $L_r$ is a reference length, taken as $L_r = L/2$. Measured angles are compared to this model with reasonable agreement in Fig. 9(a). Moreover, the static equilibrium in the tangential direction provides the constant tension gradient along the cable

$$\frac{\mathrm{d}T}{\mathrm{d}z} = m_e g D\left(\cos\theta + \frac{1}{2}\frac{\rho D L_r}{m_e}\pi C_F F_r^2 \sin\theta\right). \tag{16}$$

A dimensionless phase velocity $c_r$ may thus be predicted as

$$c_r = \frac{1}{c_o}\sqrt{\frac{T_r}{m}}, \quad T_r = \left(\frac{\mathrm{d}T}{\mathrm{d}z}\right)\frac{L_r}{D}, \quad c_o^2 = \frac{m_e g L_r}{m}. \tag{17}$$

### 4.3. Wave features

The motion angular frequency $\omega$ is measured at several spanwise locations along the cable, showing a uniform distribution, Fig. 10(a). This means that the overall cable motion has a single harmonic component. Since the cable is bent in the vertical towing plane at a constant angle $\theta$, the significant Strouhal number is derived from experiments by applying the cosine relationship of Williamson [26], $S_t = \omega/2\pi D/U\cos\theta$, and then compared to a universal $S_t(R_e)$ curve [27], Fig. 10(b). Measurements show a reasonable agreement to the general VIV phenomenology, supporting the main idea of the fluid role in

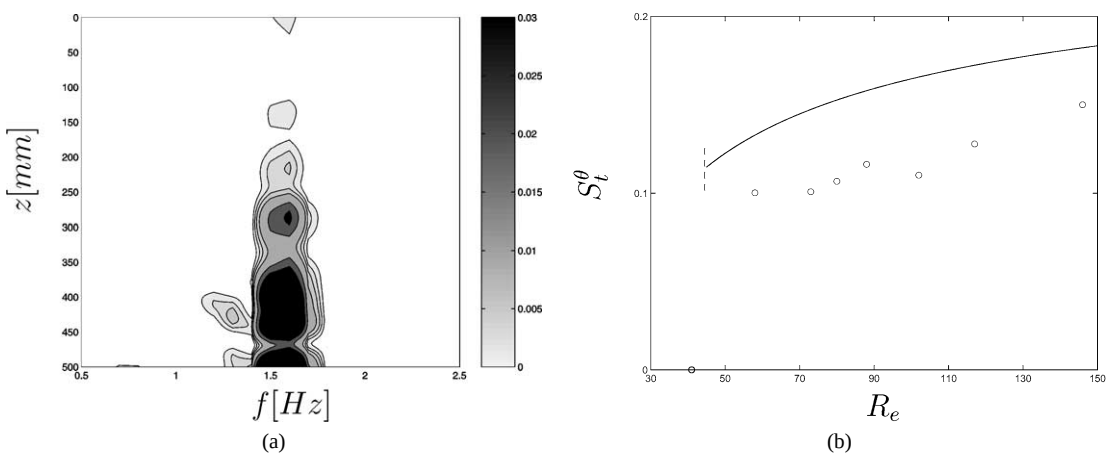


(a) (b)

Fig. 10. (a) Power Spectral Density (PSD) of the measured transverse cable displacement $y(z,t)$. (b) Strouhal number $S_t^\theta$ as a function of the Reynolds number $R_e$: ∘, experiments; —, relation $S_t = 0.2665 - 1.018/\sqrt{R_e}$ [27].

selecting the VIW angular frequency through Strouhal's law. VIW are observed as the Reynolds number is above the threshold $R_e \sim 50$ according to [27]. The measured Strouhal number is an increasing function of the Reynolds number. Note here that the cable bending angle is of about $\pi/4$, which is at the limits of the $S_t$ cosine relationship. The VIW phase velocity is measured at half of the cable length and the comparison with the model is shown in Fig. 9(b), again with reasonable agreement. This supports the main idea of the structure role in setting the VIW wavenumber, the angular frequency being fixed by Strouhal's law.

## 5. Conclusions

Vortex-induced waves (VIW) in very slender structures have been analyzed. A selection criterion for VIW frequency and wavenumber has been established by analytical arguments, then validated against numerical simulations and experimental data. The fluid selects the frequency, according to Strouhal's law, then the structure fixes the wavenumber as dictated by its dispersion relation. This approach has been validated in comparison with numerical simulations of the proposed model and with experiments. Moreover, the coupled cable-van der Pol model is found to capture most of the key features observed in DNS computations of such systems. The results on selection of frequency and wavenumber sketched in Fig. 3 may be easily extended to the case of a more complex structure model, such as Euler–Bernoulli tensioned beams with non-linear effects, which would modify the dispersion relation of the structure. The near wake vortex street is modelled by a continuous distribution of van der Pol oscillators arranged along the structure extent. Oscillators are coupled each other via the structure motion only. Spanwise interaction may also be included in order to model 3-D vortex shedding phenomena. Diffusion allows to model cellular vortex shedding from a stationary structure in shear flow [13,14,28,19]. Stiffness is required to describe oblique shedding and wave shocks by end effects at low $R_e$ from stationary structures in uniform flow [29,19]. Again, results on selection of frequency and wavenumber may be extended by including these effects in the fluid dispersion relation [30,19].

## Acknowledgement

The help of Antoine Garcia and Davi d'Elia Miranda is gratefully acknowledged for technical assistance in designing and setting up the experiment.

## References

[1] J.K. Vandiver, Dimensionless parameters important to the prediction of vortex-induced vibration of long, flexible cylinders in ocean currents, J. Fluids Structures 7 (1993) 423–455.
[2] G. Moe, Ø. Arntsen, VIV analysis of risers by complex modes, in: 11th International Offshore and Polar Engineering Conference, vol. 3, 2001, pp. 426–430.
[3] C.M. Alexander, The complex vibrations and implied drag of a long oceanographic wire in cross-flow, Ocean Engrg. 8 (4) (1981) 379–406.
[4] D.J. Newman, G.E. Karniadakis, A direct numerical simulation study of flow past a freely vibrating cable, J. Fluid Mech. 344 (1997) 95–136.
[5] C. Evangelinos, G.E. Karniadakis, Dynamics and flow structures in the turbulent wake of rigid and flexible cylinders subject to vortex-induced vibrations, J. Fluid Mech. 400 (1999) 91–124.
[6] C. Evangelinos, D. Lucor, G.E. Karniadakis, DNS-derived force distribution on flexible cylinders subject to vortex-induced vibration, J. Fluids Structures 14 (3–4) (2000) 429–440.
[7] K.F. Graff, Wave Motion in Elastic Solids, Ohio State University Press, 1975.
[8] R.W. Clough, J. Penzien, Dynamics of Structures, McGraw-Hill, 1975.
[9] R.D. Blevins, Flow-Induced Vibrations, Van Nostrand–Reinhold, 1990.
[10] S. Balasubramanian, R.A. Skop, A new twist on an old model for vortex-excited vibrations, J. Fluids Structures 11 (1997) 395–412.
[11] R.A. Skop, G. Luo, An inverse-direct method for predicting the vortex-induced vibrations of cylinders in uniform and nonuniform flows, J. Fluids Structures 15 (6) (2001) 867–884.
[12] M. Gaster, Vortex shedding from slender cones at low Reynolds numbers, J. Fluid Mech. 38 (1969) 565–576.
[13] B.R. Noack, F. Ohle, H. Eckelmann, On cell formation in vortex streets, J. Fluid Mech. 227 (1991) 293–308.
[14] S. Balasubramanian, R.A. Skop, A nonlinear oscillator model for vortex shedding from cylinders and cones in uniform and shear flows, J. Fluids Structures 10 (1996) 197–214.
[15] R.T. Hartlen, I.G. Currie, Lift-oscillator model of vortex-induced vibration, J. Engrg. Mech. Division 96 (EM5) (1970) 577–591.
[16] M.L. Facchinetti, E. de Langre, F. Biolley, Coupling of structure and wake oscillator in vortex-induced vibrations, J. Fluids Structures 2004, in press.
[17] M.S. Pantazopoulos, Vortex-induced vibration parameters: critical review, in: 17th International Conference on Offshore Mechanics Arctic Engineering, ASME, 1994, pp. 199–255.

[18] B.J. Vickery, R.D. Watkins, Flow-induced vibration of cylindrical structures, in: Proceedings of the 1st Australian Conference, University of Western Australia, 1962, pp. 213–241.
[19] M.L. Facchinetti, Un modèle phénoménologique des vibrations induites par détachement tourbillonnaire, Ph.D. thesis, École Polytechnique, Palaiseau, France, 2003.
[20] R.E.D. Bishop, A.Y. Hassan, The lift and drag forces on a circular cylinder oscillating in a flowing fluid, Proc. Roy. Soc. London Ser. A 277 (1964) 51–75.
[21] R. King, Vortex excited oscillations of yawed circular cylinders, J. Fluid Engrg. 99 (1977) 495–502.
[22] O.M. Griffin, Vortex-excited cross flow vibrations of a single cylindrical tube, in: S.S. Chen, M.D. Bernstein (Eds.), Flow-Induced Vibrations, ASME, 1980.
[23] A.P. Dowling, The dynamics of towed flexible cylinders. Part 1. Neutrally buoyant elements, J. Fluid Mech. 187 (1988) 507–532.
[24] A.P. Dowling, The dynamics of towed flexible cylinders. Part 2. Negatively buoyant elements, J. Fluid Mech. 187 (1988) 533–571.
[25] R.D. Blevins, Applied Fluid Dynamics Handbook, Van Nostrand–Reinhold, 1984.
[26] C.H.K. Williamson, Vortex dynamics in the cylinder wake, Annu. Rev. Fluid Mech. 28 (1996) 477–539.
[27] G.L. Brown, C.H.K. Williamson, A series in $1/\sqrt{R_e}$ to represent the Strouhal–Reynolds number relationship of the cylinder wake, J. Fluids Structures 12 (1998) 1073–1085.
[28] M.L. Facchinetti, E. de Langre, F. Biolley, Vortex shedding modeling using diffusive van der Pol oscillators, C. R. Mecanique 330 (2002) 451–456.
[29] P.A. Monkewitz, C.H.K. Williamson, G.D. Miller, Phase dynamics of Karman vortices in cylinder wakes, Phys. Fluids 8 (1) (1996) 91–96.
[30] M.L. Facchinetti, E. de Langre, F. Biolley, Vortex-induced waves along cables, in: 5th Symposium on Fluid-Structure Interactions, Aeroelasticity, Flow-Induced Vibrations and Noise, vol. 3, ASME, 2002.